AIMS Mathematics

AIMS Mathematics, 11(7): 21654–21673.
DOI: 10.3934/math.2026876
Received: 29 May 2026
Revised: 26 June 2026
Accepted: 30 June 2026
Published: 21 July 2026

https://www.aimspress.com/journal/Math

Research article

Vibration suppression and Hopf bifurcation control in a nonlinear rotating pendulum using time-delayed acceleration feedback

Khalid Alluhydan[1,*] and M. N. Abd EL-Salam[2]

[1] Department of Mechanical Engineering, College of Engineering, King Saud University, Riyadh 12372, Saudi Arabia
[2] Basic Sciences Department, Common First Year Deanship, King Saud University, Riyadh 12373, Saudi Arabia

* **Correspondence:** Email: kalluhydan@ksu.edu.sa.

Abstract: The nonlinear vibration characteristics of a rotating pendulum subjected to harmonic excitation were examined in this work. To mitigate excessive oscillations and improve dynamic stability, a negative delayed acceleration feedback control scheme was implemented. Approximate analytical solutions were derived near the primary resonance using the method of multiple scales, resulting in nonlinear modulation equations that govern the amplitude and phase evolution. The steady-state response and its stability were analyzed through eigenvalue-based linearization techniques. Numerical simulations employing a fourth-order Runge–Kutta algorithm were performed to verify the analytical predictions and to explore the influence of key system parameters. The effects of detuning, excitation amplitude, nonlinear modulation strength, control gain, and time delay on the system response and stability were systematically investigated. The results demonstrate that time delay significantly alters stability boundaries through Hopf bifurcations, while appropriate tuning of the delayed feedback enhances vibration suppression. A good agreement between analytical and numerical results confirms the applicability of the perturbation approach and highlights the effectiveness of delayed acceleration control in suppressing nonlinear oscillations.

Keywords: rotating pendulum; time-delayed acceleration control; primary resonance; Hopf bifurcation
Mathematics Subject Classification: 34C15, 34C46, 34F15, 70H03, 74G10

1. Introduction

Nonlinear oscillatory systems with parametric excitation have attracted sustained attention due to their complex dynamic behavior and wide range of engineering applications. Among these systems, rotating and parametrically excited pendulums represent a fundamental class of nonlinear oscillators encountered in rotating machinery, vibration absorbers, energy harvesting devices, and control systems. Owing to the combined effects of geometric nonlinearity, parametric modulation, and external forcing, such systems may exhibit resonance amplification, multi-stability, jump phenomena, and complex stability boundaries [1,2]. The rotating pendulum, in particular, has been widely studied as a canonical model for investigating nonlinear dynamic phenomena. Belyakov et al. [3] studied a pendulum with a periodically varying length, modeled as a weightless rod with a point mass moving along its axis. They derived instability boundaries near resonance, identified regions of oscillatory and rotational motions, and validated the analytical results numerically. They also investigated parameter-dependent transitions to chaotic behavior. Subsequent studies have shown that parametric excitation can significantly modify frequency–response curves and induce nonlinear effects such as bifurcations and abrupt transitions between coexisting solutions [4,5]. These features make rotating pendulum systems an ideal platform for studying nonlinear resonance and control strategies. Analytical approaches based on perturbation techniques have proven particularly effective for investigating the response of weakly nonlinear systems near resonance. The method of multiple scales has been extensively used to derive amplitude–phase modulation equations and frequency–response relations for parametrically excited oscillators [6–9]. Extensions of these techniques to systems with small delays and nonlinear feedback have further enriched the understanding of slow-flow dynamics and stability behavior [10]. Such analytical frameworks provide valuable insight into resonance mechanisms and allow for systematic stability analysis. The time delay is an effective tool for enhancing stability and regulating nonlinear vibrations in dynamic systems [11–14]. It can reduce oscillation amplitudes, prevent undesired behavior, and influence bifurcation points, enabling controlled transitions between stable and unstable states. Combined with classical controllers like a proportional-derivative (PD) or proportional–integral–derivative (PID), time-delayed control improves the overall performance and vibration suppression of complex systems. Amer et al. [15] demonstrated that position and velocity time-delay feedback provides an effective mechanism for suppressing vibrations in a hybrid Rayleigh–Van der Pol–Duffing oscillator. Stability analysis reveals that the system is highly sensitive to delay parameters and feedback gains, where inappropriate choices may induce Hopf bifurcation and destabilize the system. Naser et al. [16] investigated the effects of a time-delayed controller on the static bifurcations and nonlinear oscillations of a self-excited system using both 2D and 3D visualizations. The combined use of 2D and 3D plots provided deeper insight into the interaction between system parameters, offering a clearer understanding of the stability regions and nonlinear response. The time delay was shown to effectively improve the vibration suppression and stability of the dielectric elastomer circular membrane under the PD controller. The onset of nonlinear oscillations was influenced, and the membrane's performance was enhanced through proper tuning of the PD gains and delay [17]. Wenjie et al. [18] examined a diffusive Leslie–Gower model with prey Allee effect and predator fear effect. They derive the characteristic equations, investigate the conditions for the occurrence of Turing–Hopf bifurcations, which represent diffusion-induced spatial patterns and temporal population oscillations, and verify the analytical results through numerical simulations. In the control field, negative acceleration feedback plays a crucial role in enhancing the stability and performance of dynamic systems [19–22], particularly in vibration control applications. Kaslik et al. [23] showed that distributed delays strongly influence system stability and can trigger or suppress Hopf bifurcations, leading to changes in oscillatory behavior. Their findings highlight the important role of delayed interactions in neural dynamics. By feeding back a signal proportional to the system's acceleration with an opposing (negative) effect, this technique effectively reduces oscillation amplitudes and suppresses unwanted high-frequency responses. It improves damping characteristics without significantly altering the system's natural frequency, making it especially useful in mechanical and structural systems. Mokni et al. [24] analyzed a Darwinian Ricker system, revealing Neimark–Sacker, period-doubling, and codimension-two bifurcations (1:2, 1:3, 1:4 resonances) via bifurcation and center manifold theories. Numerical simulations confirm chaotic dynamics. The study highlights how immigration and strong Allee effects drive complex population behaviors, with key implications for ecological forecasting under environmental change.

Chatterjee [25] demonstrated that recursive time-delayed acceleration feedback is an effective and flexible strategy for suppressing vibrations in dynamic systems. By recursively incorporating multiple delayed acceleration terms, the control scheme significantly enhances damping and reduces oscillation amplitudes over a wide range of operating conditions. The single-degree-of-freedom damped oscillator is a key model in vibration control, where the delayed acceleration derivative is highly effective [26]. It was found that certain delay combinations, especially when the acceleration delay is twice the velocity delay, provide a larger stability region. Moreover, delayed positive acceleration feedback offers better performance than negative feedback, enhancing stability and delaying the onset of Hopf bifurcation.

In the present work, the nonlinear dynamic behavior of a rotating pendulum subjected to external harmonic forcing is systematically investigated in the presence of time-delayed acceleration feedback control. The study begins with the formulation of the mathematical model and the incorporation of the delayed strategy. Then, the method of multiple scales is applied to derive the approximate analytical solutions and obtain the amplitude-phase modulation equations near the primary resonance. The steady-state response and frequency-response relationships are subsequently developed, followed by a detailed stability analysis using linearization and eigenvalue techniques. To validate the analytical findings, numerical simulations based on the fourth-order Runge–Kutta method are performed. Furthermore, the effects of key system parameters, including detuning, forcing amplitude, nonlinear modulation, control gain, and time delay, are thoroughly examined. Finally, the main conclusions regarding vibration suppression and stability enhancement are presented.

2. Model description

A rigid pendulum of length l and mass m is hinged at a fixed pivot and undergoes planar motion under the influence of gravity. The system is subjected to an external harmonic force of the form $f\cos(\Omega t)$, applied at the pivot as presented in Figure 1(a). To capture nonlinear elastic effects, a torsional stiffness is introduced, such that the restoring torque depends on the angular displacement $\varphi(t)$ according to $k(x) = k_0(1 - \beta\, cos\varphi)$, where k_0 is the linear stiffness coefficient, and β is a dimensionless parameter characterizing the strength of the stiffness modulation. The motion of the nonlinear rotating pendulum is formulated using Lagrange's equations. The kinetic energy of the system is defined as:

$$T = \frac{1}{2} ml^2 \dot{\varphi}^2. \tag{1}$$

To incorporate the nonlinear restoring effect, the potential energy is formulated in a modified form such that the resulting restoring torque takes the form $(1 - \beta \cos\varphi)\sin\varphi$. This expression is obtained by the potential energy as follows:

$$V(\varphi) = -\cos\varphi - \frac{\beta}{2} \sin^2 \varphi. \tag{2}$$

The Lagrangian of the system is defined as

$$L(\varphi) = T(\varphi) - V(\varphi) = \frac{1}{2} ml^2 \dot{\varphi}^2 + \cos\varphi + \frac{\beta}{2} \sin^2 \varphi. \tag{3}$$

Applying the Euler–Lagrange equation,

$$\frac{d}{dt}\left(\frac{\partial L}{\partial \dot{\varphi}}\right) - \frac{\partial L}{\partial \varphi} = Q, \tag{4}$$

where Q represents the generalized external force as

$$Q = F \cos(\Omega t), \tag{5}$$

where F and Ω denote the amplitude and frequency of excitation, respectively. Substituting into the Euler–Lagrange equation (4),

$$ml^2 \ddot{\varphi} + (1 - \beta \cos\varphi) \sin\varphi = F \cos(\Omega\, t). \tag{6}$$

In the given equation, the term $ml^2\ddot{\varphi}$ corresponds to the inertial torque from the pendulum angular acceleration. The $(1 - \beta \cos\varphi) \sin\varphi$ represents the nonlinear restoring torque, where the parameter β governs the degree of stiffness nonlinearity in the system. On the right-hand side, $F \cos(\Omega\, t)$ denotes an external harmonic excitation torque, with F and Ω representing the excitation amplitude and frequency, respectively. The quantities m, l, and φ denote the pendulum's mass, length, and angular displacement. Overall, the equation captures the dynamic equilibrium among the pendulum's inertial response, the nonlinear restoring effects, and the periodic external forcing. By dividing Eq (6) by the inertia term ml^2, a normalized form is obtained in which the coefficient of the acceleration term becomes unity. Accordingly, the forcing amplitude is rescaled by $f = \frac{F}{ml^2}$. The equation of motion can then be expressed in a dimensionless form as follows:

$$\ddot{\varphi} + (1 - \beta \cos\varphi) \sin\varphi = f \cos(\Omega\, t). \tag{7}$$

When $\beta = 0$, the model reduces to a classical forced pendulum. However, the additional term $(1 - \beta \cos\varphi)$ introduces a higher level of nonlinearity, rendering the system more comparable to a Duffing-type or parametrically excited pendulum. As a result, the governing equation is capable of exhibiting multiple equilibrium states, bifurcation phenomena, and potentially chaotic dynamics. To suppress the vibrations of the rotating pendulum, a negative delayed acceleration control is employed, as illustrated in Figure 1(b). Delayed acceleration control is an active vibration control strategy in which the control force is generated using the time-delayed acceleration feedback of the system. Unlike conventional acceleration feedback, the inclusion of a time delay introduces a phase shift that can be exploited to enhance vibration suppression and stability. In practice, the delayed acceleration signal

$\ddot{\varphi}(t-\tau)$ can be obtained using accelerometers or inertial measurement units (IMUs) sensors and implemented through a digital delay unit. To reduce measurement noise, standard filtering techniques such as low-pass or Kalman filters may be employed. In this study, ideal measurements are assumed to evaluate the theoretical effectiveness of the proposed controller, although its practical implementation can readily incorporate filtering and state-estimation methods. In its general form, the delayed acceleration control force is expressed as

$$F(t) = -\gamma\ddot{\varphi}(t-\tau), \tag{8}$$

where γ denotes the feedback gain, and τ represents the time delay. The negative sign indicates that the control action is designed to oppose the system motion, thereby dissipating vibrational energy. Accordingly, Eq (7) can be rewritten in the following form:

$$\ddot{\varphi} + (1-\beta\cos\varphi)\sin\varphi = f\cos\Omega t - \gamma\ddot{\varphi}(t-\tau). \tag{9}$$

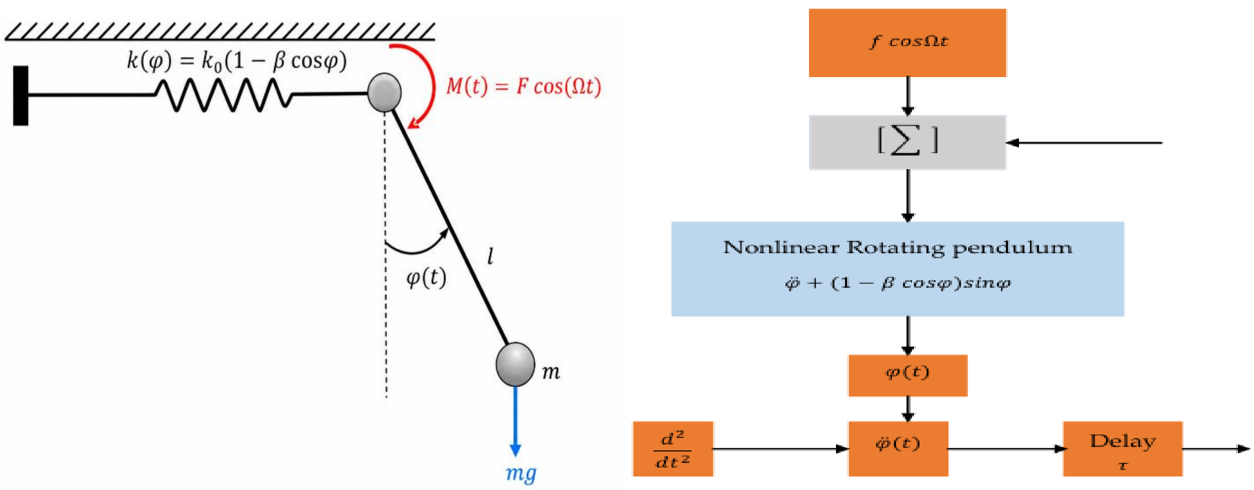

(a) (b)

Figure 1. (a) Schematic model of the rotating pendulum, and (b) closed-loop diagram of the controlled rotating pendulum system with negative acceleration time-delayed feedback.

3. Autonomous amplitude–phase equations

In order to apply the method of multiple scales to derive an approximate solution to Eq (9), the nonlinear functions ($\sin\varphi$ and $\cos\varphi$) are expressed in terms of their Maclaurin series expansions as follows:

$$\ddot{\varphi} + (1-\beta)\varphi + \left(\frac{4\beta-1}{6}\right)\varphi^3 - \left(\frac{\beta}{12}\right)\varphi^5 = f\cos\Omega t - \gamma\ddot{\varphi}(t-\tau). \tag{10}$$

For the sake of simplification, parameters are defined as $\omega = \sqrt{1-\beta}, \delta_1 = (4\beta-1)/6$, and $\delta_2 = \beta/12$. With these substitutions, Eq (10) takes the form

$$\ddot{\varphi} + \omega^2\varphi + \delta_1\varphi^3 - \delta_2\varphi^5 = f\cos\Omega t - \gamma\ddot{\varphi}(t-\tau). \tag{11}$$

Using the perturbation technique, a first-order approximate solution to the equation of motion of the rotating pendulum is obtained in the following form [7,8]:

$$\varphi(t,\varepsilon)=\varphi_0(T_0,T_1\ )+\varepsilon\varphi_1(T_0,T_1\ )+O(\varepsilon^2), \tag{12}$$

where ε is the perturbation parameter, $T_0=t$, and $T_1=\varepsilon\, t$. Accordingly, with respect to the time scales T_0, and T_1, the time derivatives d/dt and $d^2/d\,t^2$ can be expressed as

$$\begin{cases}\frac{d}{dt}=\frac{\partial}{\partial T_0}+\varepsilon\frac{\partial}{\partial T_1}+\ldots\\ \frac{d^2}{dt^2}=\frac{\partial^2}{\partial T_0^2}+2\varepsilon\left(\frac{\partial}{\partial T_0}\right)\left(\frac{\partial}{\partial T_1}\right)+\ldots\end{cases}. \tag{13}$$

To carry out the solution steps, the system parameters may be appropriately scaled such that they are of comparable order, which facilitates the application of the perturbation method and simplifies the subsequent analytical derivations.

$$\delta_1=\varepsilon\tilde{\delta}_1,\delta_2=\varepsilon\tilde{\delta}_2,f=\varepsilon\tilde{f},\gamma=\varepsilon\tilde{\gamma}. \tag{14}$$

Inserting Eqs (12)–(14) into Eq (11) and then equating the coefficients of like powers of ε yields the zeroth-order problem, $O(\varepsilon^0)$.

$$\frac{\partial^2\varphi_0}{\partial T_0^2}+\omega^2\varphi_0=0. \tag{15}$$

And the first-order problem, $O(\varepsilon)$.

$$\frac{\partial^2\varphi_1}{\partial T_0^2}+\omega_1^2\varphi_1=-2\frac{\partial}{\partial T_1}\left(\frac{\partial\varphi_0}{\partial T_0}\right)-\tilde{\delta}_1\varphi_0^3+\tilde{\delta}_2\varphi_0^5+\tilde{f}\cos\Omega\, t-\tilde{\gamma}\frac{\partial^2\varphi_0(t-\tau)}{\partial T_0^2}. \tag{16}$$

Equation (15) is a homogeneous second-order differential equation, and its solution takes the form

$$\varphi_0(T_0,T_1\ )=A(T_1)\,e^{i\omega T_0}+\bar{A}(T_1)\,e^{-i\omega T_0}\ . \tag{17}$$

From Eq (17), we have

$$\begin{cases}\varphi_0(T_0-\tau)=A(T_1-\varepsilon\tau)e^{i\omega T_0}\,e^{-i\omega\tau}+\bar{A}(T_1-\varepsilon\tau)e^{-i\omega T_0}\,e^{i\omega\tau}\\ \frac{\partial\varphi_0(T_0-\tau)}{\partial T_0}=i\omega A(T_1-\varepsilon\tau)e^{i\omega T_0}\,e^{-i\omega\tau}-i\omega\bar{A}(T_1-\varepsilon\tau)e^{-i\omega T_0}\,e^{i\omega\tau}\\ \frac{\partial^2\varphi_0(T_0-\tau)}{\partial T_0^2}=-\omega^2A(T_1-\varepsilon\tau)e^{i\omega T_0}\,e^{-i\omega\tau}-\omega^2\bar{A}(T_1-\varepsilon\tau)e^{-i\omega T_0}\,e^{i\omega\tau}\end{cases}. \tag{18}$$

By using Taylor expansion, $A(T_1-\varepsilon\tau)\approx A(T_1)$. Note that the unknown function $A(T_1)$ will be determined later, and $i=\sqrt{-1}$. Substituting Eqs (17) and (18) into the right-hand side of Eq (16) yields the first-order approximation in the following form:

$$\frac{\partial^2\varphi_1}{\partial T_0^2}+\omega^2\varphi_1=\left(\frac{\tilde{f}}{2}\right)e^{i\Omega T_0}+\left(-2i\omega\frac{\partial A}{\partial T_1}-3\tilde{\delta}_1A^2\bar{A}+10\tilde{\delta}_2A^3\bar{A}^2-\omega^2\tilde{\gamma}Ae^{-i\omega\tau}\right)e^{i\omega T_0}$$

$$-\left(\tilde{\delta}_1A^3-5\tilde{\delta}_2A^4\bar{A}\right)e^{3i\omega T_0}+\left(\tilde{\delta}_2A^5\right)e^{5i\omega T_0}+cc, \tag{19}$$

where cc is the complex conjugate term. For the particular solution of Eq (19) to remain bounded, all secular terms must be eliminated, such that

$$\varphi_1(T_0, T_1) = \left(\frac{\tilde{f}}{2\omega_1^2 - 2\Omega^2}\right) e^{i\Omega T_0} + \left(\frac{\tilde{\delta}_1 A^3 - 5\tilde{\delta}_2 A^4 \bar{A}}{8\omega_1^2}\right) e^{3i\omega T_0} - \left(\frac{\tilde{\delta}_2 A^5}{24\omega_1^2}\right) e^{5i\omega T_0} + cc. \quad (20)$$

To obtain the solvability conditions from the first-order approximation at the primary resonance case (i.e., $\Omega \approx \omega$), a detuning parameter σ is introduced to quantify the closeness of Ω to ω as follows:

$$\Omega = \omega + \sigma = \omega + \varepsilon\tilde{\sigma}; \sigma = \varepsilon\tilde{\sigma}. \quad (21)$$

Inserting Eq (21) into Eq (19), we can present the solvability conditions of Eq (19) as follows:

$$-2i\omega \frac{\partial A}{\partial T_1} - 3\tilde{\delta}_1 A^2 \bar{A} + 10\tilde{\delta}_2 A^3 \bar{A}^2 - \omega^2 \tilde{\gamma} A e^{-i\omega\tau} + \frac{\tilde{f}}{2} e^{i\tilde{\sigma} T_1} = 0, \quad (22)$$

$$\frac{\partial A}{\partial T_1} = \frac{3i\tilde{\delta}_1}{2\omega} A^2 \bar{A} - \frac{5i\tilde{\delta}_2}{\omega} A^3 \bar{A}^2 + \frac{i\omega\tilde{\gamma}}{2} A e^{-i\omega\tau} - \frac{i\tilde{f}}{4\omega} e^{i\tilde{\sigma} T_1}. \quad (23)$$

To derive the slow-flow modulation equations of the investigated rotating pendulum, the unknown complex amplitude $A(T_1)$ is expressed in polar (amplitude–phase) form as follows [20]:

$$A(T_1) = \frac{1}{2} a(T_1)\, e^{\theta(T_1)}, \quad (24)$$

where $a(T_1)$ denotes the real, slowly varying oscillation amplitude, and $\theta(T_1)$ represents the corresponding phase. This transformation facilitates the separation of the real and imaginary parts of the governing equations, enabling the derivation of the slow-flow (modulation) equations that describe the evolution of amplitude and phase on the slow time scales. According to the definition of the first derivative in Eq (13),

$$\frac{dA}{dt} = \varepsilon \frac{\partial A}{\partial T_1} + O(\varepsilon^2). \quad (25)$$

Inserting Eqs (23) and (24) into Eq (25),

$$\left(\dot{a} + ia\dot{\theta}\right) = \varepsilon\left(\frac{3i\tilde{\delta}_1}{2\omega} A^2 \bar{A} - \frac{5i\tilde{\delta}_2}{\omega} A^3 \bar{A}^2 + \frac{i\omega\tilde{\gamma}}{2} A e^{-i\omega\tau} - \frac{i\tilde{f}}{4\omega} e^{i\tilde{\sigma} T_1}\right). \quad (26)$$

Back to the main system parameters with the help of Eq (14) yields

$$\left(\dot{a} + ia\dot{\theta}\right) = \frac{3i\delta_1}{8\omega} a^3 - \frac{5i\delta_2}{64\omega} a^5 + \frac{i\omega\gamma}{2} a e^{-i\omega\tau} - \frac{if}{2\omega} e^{i\phi}. \quad (27)$$

Now, by separating the real and imaginary parts, the following nonlinear autonomous dynamical system governing the slow evolution of the amplitude and phase is obtained as:

$$\dot{a} = \frac{\omega\gamma}{2} a \sin(\omega\tau) + \frac{f}{2\omega} \sin\phi, \quad (28)$$

$$a\dot{\theta} = \frac{3\delta_1}{8\omega} a^3 - \frac{5\delta_2}{64\omega} a^5 + \frac{\omega\gamma}{2} a \cos(\omega\tau) - \frac{f}{2\omega} \cos\phi, \quad (29)$$

where $\phi = \sigma t - \theta$, so Eq (29) can be written as

$$a\dot{\phi} = \sigma a - \frac{3\delta_1}{8\omega}a^3 + \frac{5\delta_2}{64\omega}a^5 - \frac{\omega\gamma}{2}a\cos(\omega\tau) + \frac{f}{2\omega}\cos\phi. \tag{30}$$

The vibration amplitude of the rotating pendulum is represented by $a(t)$, while ϕ denotes the phase angle of motion. The steady-state amplitude and phase of the vibrating system are obtained by imposing the equilibrium conditions of the slow-flow equations,

$$\dot{a} = 0, \dot{\phi} = 0, \tag{31}$$

which implies that $\dot{\theta} = \sigma$. Consequently, the modulation equations reduce to a set of nonlinear algebraic equations governing the steady-state response of the system, expressed as

$$\frac{f}{2\omega}\sin\phi = -\frac{\omega\gamma}{2}a\sin(\omega\tau), \tag{32}$$

$$\frac{f}{2\omega}\cos\phi = -\frac{5\delta_2}{64\omega}a^5 + \frac{3\delta_1}{8\omega}a^3 + \frac{\omega\gamma}{2}a\cos(\omega\tau) - \sigma a. \tag{33}$$

These nonlinear algebraic equations determine the steady-state vibration amplitude and phase angle of the rotating pendulum and are subsequently used to analyze the response characteristics and stability of the system. To obtain the frequency–response equation, Eqs (32) and (33) are squared and summed, which yields

$$\left(-\frac{5\delta_2}{64\omega}a^5 + \frac{3\delta_1}{8\omega}a^3 + \frac{\omega\gamma}{2}a\cos(\omega\tau) - \sigma a\right)^2 + \left(\frac{\omega\gamma}{2}a\sin(\omega\tau)\right)^2 = \left(\frac{f}{2\omega}\right)^2. \tag{34}$$

After simplification, this procedure eliminates the phase angle ϕ, leading to a single nonlinear algebraic equation that relates the steady-state vibration amplitude a to the detuning parameter σ and the system parameters. This equation represents the frequency–response relation of the rotating pendulum and is used to investigate resonance behavior, jump phenomena, and stability characteristics.

3.1. Equilibrium response and stability conditions

To investigate the stability of the steady-state solution, the following perturbation form is introduced:

$$\begin{cases} a = a_0 + a_1 \\ \phi = \phi_0 + \phi_1 \end{cases}, \tag{35}$$

where a_0 and ϕ_0 denote the equilibrium non-trivial solutions of Eqs (32) and (33), respectively. The variables a_1 and ϕ_1 represent small perturbations about the equilibrium state, satisfying that,

$$\begin{cases} |a_1| << |a_0| \\ |\phi_1| << |\phi_0| \end{cases}. \tag{36}$$

Inserting Eq (35) into Eqs (28) and (30) and linearizing about the equilibrium point leads to the following system of linearized equations:

$$\dot{a}_1 = \left(\frac{\omega\gamma}{2}\sin(\omega\tau)\right)a_1 + \left(\frac{f}{2\omega}\cos\phi_0\right)\phi_1, \tag{37}$$

$$\dot{\phi}_1 = \left(\frac{\sigma}{a_0} - \frac{9\delta_1}{8\omega} a_0 + \frac{25\delta_2}{64\omega} a_0^3 - \frac{\omega\gamma}{2a_0} cos(\omega\tau)\right) a_1 - \left(\frac{f}{2\omega a_0} sin\,\phi_0\right) \phi_1. \tag{38}$$

The eigenvalues of the linearized system are determined from the characteristic determinant given by

$$\begin{vmatrix} \lambda - \frac{\omega\gamma}{2} sin(\omega\tau) & \frac{f}{2\omega} cos\,\phi_0 \\ \frac{\sigma}{a_0} - \frac{9\delta_1}{8\omega} a_0 + \frac{25\delta_2}{64\omega} a_0^3 - \frac{\omega\gamma}{2a_0} cos(\omega\tau) & \lambda + \frac{f}{2\omega a_0} sin\,\phi_0 \end{vmatrix} = 0. \tag{39}$$

Leading to the following characteristic polynomial:

$$\lambda^2 + \Gamma_1\lambda + \Gamma_2 = 0, \tag{40}$$

where

$$\begin{cases} \Gamma_1 = \dfrac{f\,sin\,\phi_0}{2\omega a_0} - \dfrac{\omega\gamma\,sin(\omega\tau)}{2} \\ \Gamma_2 = \dfrac{9\delta_1 f\,cos\,\phi_0}{16\omega^2} a_0 - \dfrac{25\delta_2 f\,cos\,\phi_0}{128\omega^2} a_0^3 + \dfrac{\omega\gamma\,cos(\omega\tau) f\,cos\,\phi_0}{4\omega a_0} - \dfrac{\sigma f\,cos\,\phi_0}{2\omega a_0}. \end{cases}$$

The roots of this equation determine the dynamic behavior and stability of the system and can be expressed as

$$\lambda_{1,2} = \frac{-\Gamma_1 \pm \sqrt{\Gamma_1^2 - 4\Gamma_2}}{2}. \tag{41}$$

The stability of the system depends mainly on the signs and values of the coefficients Γ_1 and Γ_2. The system remains stable when both coefficients are positive, $\Gamma_1 > 0$, and $\Gamma_2 > 0$, since under these conditions, the eigenvalues possess negative real parts, causing the response to diminish gradually with time. A critically stable state occurs when the discriminant satisfies $\Gamma_1^2 - 4\Gamma_2 = 0$, where the two roots coincide, and the system exhibits a rapid non-oscillatory behavior. In contrast, when $\Gamma_1^2 - 4\Gamma_2 < 0$, the eigenvalues become complex conjugates, resulting in damped oscillations. However, instability arises whenever at least one eigenvalue has a positive real part, which can occur if $\Gamma_1 \leq 0$ or $\Gamma_2 \leq 0$. Hence, the interplay between Γ_1 and Γ_2 governs the overall dynamic stability of the system.

4. Numerical investigation

To complement the analytical developments, the governing nonlinear equation of motion is integrated numerically in the time domain using a classical fourth-order Runge–Kutta scheme according to the MATLAB dde23 package. This method provides adequate accuracy and numerical stability for capturing the transient and steady-state responses of strongly nonlinear oscillatory systems. Simulations are conducted under worst-case resonance conditions to assess the effectiveness of the proposed control strategy. Time histories, phase portraits, and amplitude–frequency responses are extracted to validate analytical predictions and to examine the influence of system parameters on the dynamic behavior, for the following parameter values: $\beta = 0.2, f = 0.13, \tau = 1.5$, and $\gamma = 0.5$.

4.1. Uncontrolled model

Figure 2 illustrates the dynamic behavior of the uncontrolled system. The time-history response shown in Figure 2(a) reveals that the oscillation amplitude persists over time without noticeable decay. After the initial transient, the response stabilizes into sustained oscillations with nearly constant amplitude, indicating the absence of inherent damping or any active control mechanism. This behavior is characteristic of nonlinear systems operating near resonance, where continuous energy exchange among system components prevents natural attenuation of vibrations. The corresponding phase portrait in Figure 2(b) further confirms this behavior. The trajectories in the amplitude–velocity plane form closed, non-convergent loops, representing a stable limit cycle. The lack of convergence toward the equilibrium point indicates that the system does not exhibit asymptotic stability. Moreover, the symmetry and regularity of the closed orbits suggest periodic and non-chaotic motion under the selected parameter values.

4.2. Controlled model

The system response after applying the negative acceleration control is depicted in Figure 3. As shown in Figure 3(a), the oscillation amplitude is significantly reduced compared with the uncontrolled case, and the transient response decays rapidly toward the equilibrium state. This behavior demonstrates that the control strategy effectively introduces damping into the system, enabling efficient dissipation of vibrational energy. As time increases, the response converges smoothly to a near-zero steady state, indicating asymptotic stability and successful suppression of sustained nonlinear oscillations. Figure 3(b) presents the corresponding phase portrait. Unlike the closed limit-cycle trajectories observed in the uncontrolled system, the phase trajectories now spiral inward toward the origin. This inward convergence signifies the elimination of the limit cycle and stabilization of the equilibrium point. The smooth and regular nature of the spiraling trajectories indicates that the controlled system operates in a stable and non-chaotic regime. Figure 4 illustrates the dynamic response of the system under the negative delayed acceleration control strategy. The time-history response shown in Figure 4(a) spans a long time interval and exhibits relatively large oscillations at early times due to transient effects immediately following control activation. As time progresses, the oscillation amplitude gradually decreases and converges toward zero. This progressive decay confirms that the delayed control introduces an effective damping mechanism, leading to continuous energy dissipation and complete suppression of oscillations. The absence of residual vibrations at large times indicates asymptotic stability of the controlled equilibrium. The corresponding phase portrait in Figure 4(b) shows spiral trajectories with decreasing radius that converge toward the origin. This inward spiraling behavior is characteristic of a stable focus, demonstrating simultaneous decay of both amplitude and velocity. The smooth contraction of the phase trajectories indicates that the control stabilizes the system without inducing additional instabilities, oscillatory overshoot, or irregular dynamics.

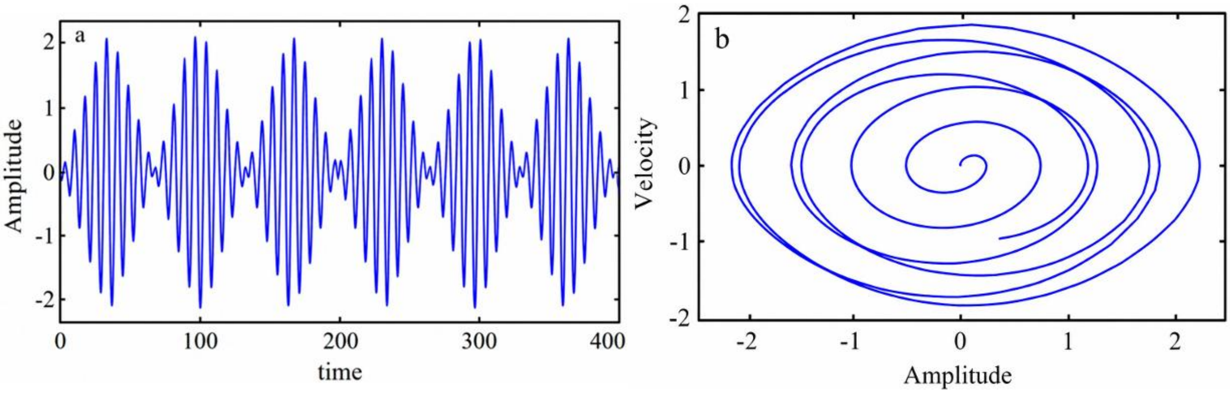

Figure 2. Dynamic behavior of the uncontrolled system. (a) Time-history response and (b) phase portrait.

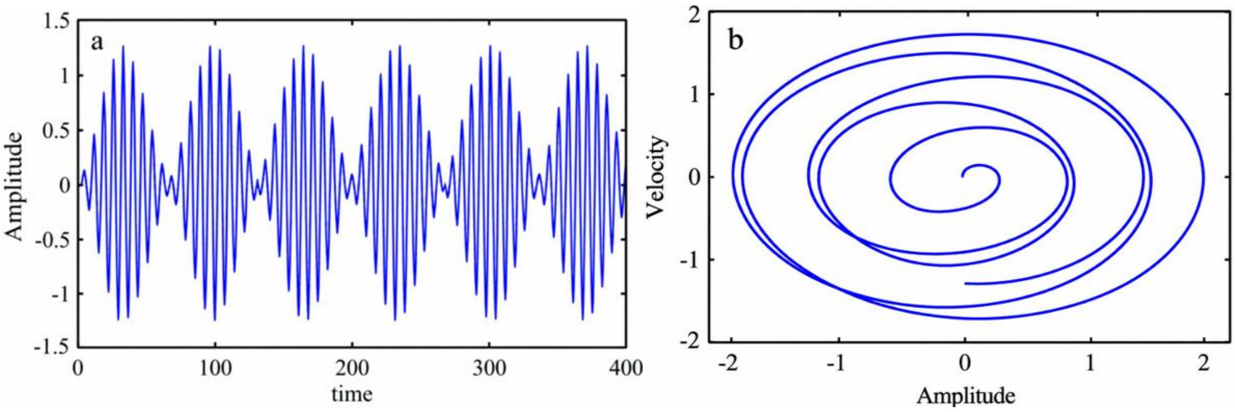

Figure 3. System response under negative acceleration control. (a) Time-history response and (b) phase portrait.

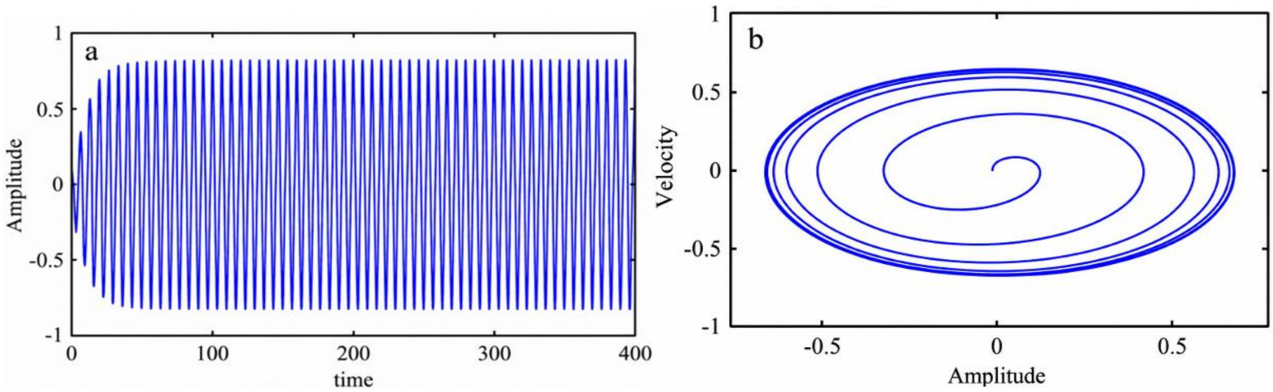

Figure 4. System response under negative delayed acceleration control. (a) Time-history response and (b) phase portrait.

4.3. Parametric effects on system response

Equation (34) was solved numerically to obtain the amplitude response as a function of the detuning parameter, which is represented in Figure 5(a). The resulting amplitude–frequency curves illustrate the dependence of the response amplitude a on the detuning parameter σ. A pronounced and symmetric peak is observed at the primary resonance case ($\sigma = 0$), where the amplitude attains its maximum value, indicating a resonance condition of the system. As $|\sigma|$ increases away from zero, the amplitude decreases rapidly and approaches zero, demonstrating strong attenuation of the system response outside the critical regime. The smooth and even symmetry of the curve with respect to $\sigma = 0$ suggests that the governing dynamics depend on σ through even-order terms (as illustrated in Eq (33)), reflecting identical behavior for positive and negative deviations from the critical point. Figure 5(b) illustrates the response curves of the controlled system for different values of the strength of the nonlinear rotating pendulum β. Increasing β leads to a higher maximum amplitude at $\sigma = 0$. For a smaller β, the response is weaker and more spread out over a wider range of σ. Figure 5(c) illustrates the equilibrium response and stability characteristics of the system in the (σ, a) plane for different values of the external forcing amplitude f. Three cases are presented, corresponding to $f = 0.09, 0.13$, and 0.17, allowing for a direct comparison of forcing effects on the system's equilibrium structure and stability. For each value of f, the equilibrium response exhibits a nonlinear dependence on the detuning parameter σ. As σ varies from negative to positive values, the equilibrium amplitude initially remains small and then increases, forming a characteristic nonlinear response curve. Increasing the forcing amplitude f results in an overall upward shift of the equilibrium branches, indicating that stronger excitation leads to higher steady-state amplitudes across the entire detuning range. As the forcing amplitude f increases from 0.09 to 0.17, the width of the multi-stability region expands, and the distance between the fold points becomes larger. This indicates that higher forcing intensifies the system's nonlinearity and increases susceptibility to jump phenomena. Figure 5(d) presents the response curves of the system for different values of the control parameter γ. Three response curves are shown, corresponding to $\gamma = 0.15, 0.2$, and 0.30, allowing for a direct assessment of how variations in γ influence the system's nonlinear response characteristics. For all values of γ, the equilibrium amplitude exhibits a nonlinear dependence on the detuning parameter. As σ varies from negative to positive values, the amplitude initially remains small, increases progressively, and then decreases, forming a characteristic nonlinear resonance-type response curve. This behavior reflects the combined effects of detuning and nonlinear stiffness on the steady-state dynamics of the system. A clear trend is observed as the control parameter γ increases. Specifically, increasing γ leads to a pronounced reduction in the equilibrium amplitude across the entire range of σ. The response curve corresponding to $\gamma = 0.30$ lies consistently below those for $\gamma = 0.20$ and $\gamma = 0.15$, indicating that larger values of γ suppress the system response more effectively. This demonstrates the stabilizing influence of γ and its role in limiting excessive oscillation amplitudes.

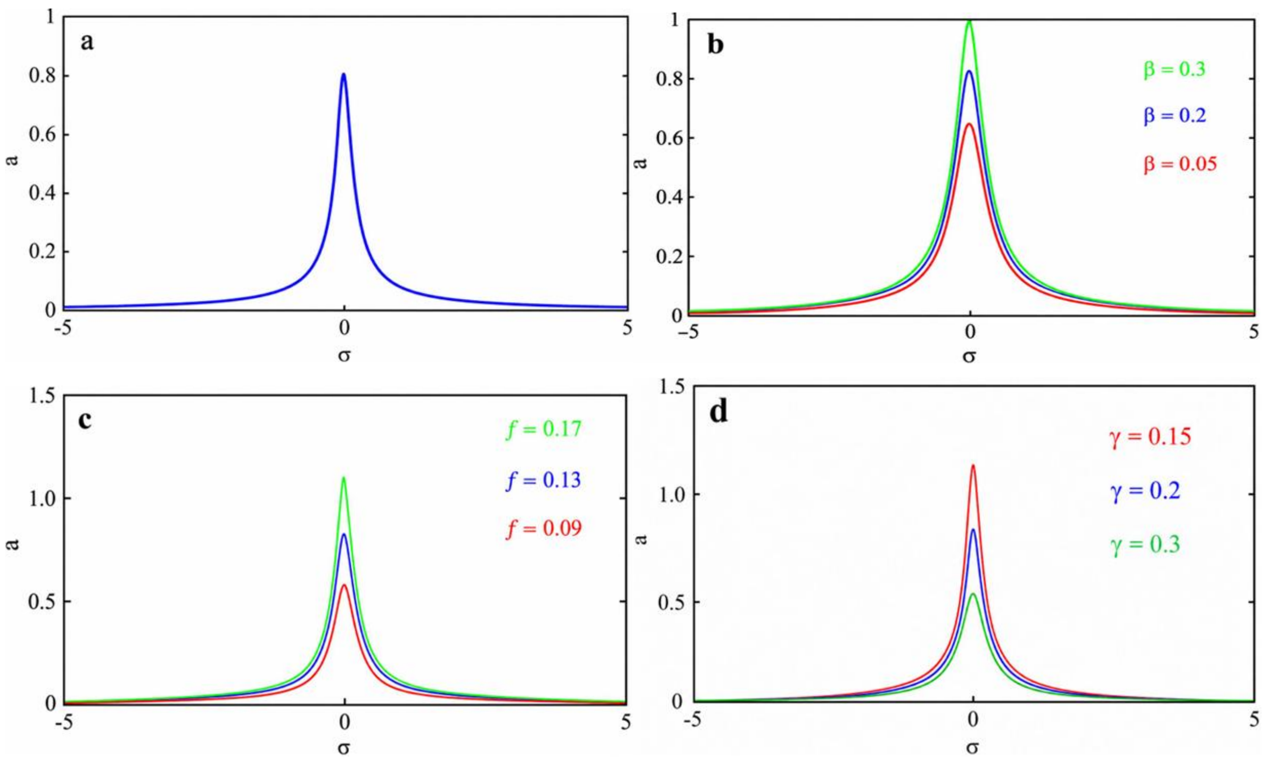

Figure 5. Response amplitude and equilibrium characteristics under variations of (a) detuning parameter σ, (b) the strength of the nonlinear rotating pendulum β, (c) forcing amplitude f, and (d) control parameter γ.

4.4. Stability analysis in the presence of time delay

We investigate the effect of time delay on the stability of the system. By incorporating a delayed acceleration feedback term, the characteristic equations are modified. The analysis reveals how time delay can shift stability boundaries, induce oscillatory instabilities, or enhance damping, providing insights into the design and tuning of delay-based control strategies. Figure 5 presents the stability diagram of the system in the (τ, a) plane. The solid red curve on the left defines the boundary of asymptotic stability, while the dashed red curve on the right corresponds to the instability boundary. Two vertical black lines indicate the critical delay values $\tau_1 = 3.13$ and $\tau_2 = 3.892$. For $0 < \tau < \tau_1$, the equilibrium point is asymptotically stable, with all characteristic roots satisfying $Re(\lambda) < 0$. In this regime, the system returns smoothly to equilibrium without oscillatory behavior; hence, it is denoted as the stable region. At the first critical point $(\tau_1, a_1) \approx (3.13,1.107)$, a pair of complex conjugate eigenvalues crosses the imaginary axis, $Re(\lambda) = 0$, indicating the occurrence of a Hopf bifurcation. Consequently, the equilibrium loses stability and self-sustained periodic oscillations begin to emerge. For $\tau_1 < \tau < \tau_2$, the system enters a transition region in which stability depends sensitively on the equilibrium amplitude a. In this interval, conditional stability may occur, and the system can exhibit delay-induced oscillations or coexistence of multiple solutions. At the second critical point $(\tau_2, a_2) \approx (3.892,1.121)$, another crossing of characteristic roots takes place, leading to a complete loss of equilibrium stability. For $\tau > \tau_2$, at least one characteristic root satisfies $Re(\lambda) > 0$, and the system evolves into an unstable regime characterized by persistent oscillations or divergent responses. This domain is therefore identified as the unstable region. The stability characteristics of the equilibrium solutions in the presence of time delay are investigated by examining the influence of key system parameters, namely the strength of the nonlinear rotating pendulum β, the external forcing amplitude f, and the control parameter γ. The results are summarized in Figure 7. For different values of the strength of the nonlinear rotating pendulum $\beta = 0.35, 0.30$, and 0.25, Figure 7(a) shows that the equilibrium solution remains stable in the absence of delay ($\tau \approx 0$). As the time delay increases, each stable equilibrium branch intersects an unstable branch at a critical delay value τ_c , indicating the occurrence of a Hopf bifurcation. At this bifurcation point, the equilibrium loses stability, and oscillatory behavior emerges. It is further observed that increasing β shifts the stability boundary toward smaller values of τ, implying that stronger feedback accelerates the onset of delay-induced instability. Figure 7(b) highlights a delay-dominated stability boundary characterized by a vertical critical line at $\tau_c = 3.52$. This result demonstrates that the onset of instability is governed exclusively by the time delay and is independent of both the equilibrium amplitude a and the external forcing amplitude f. Variations in f only induce vertical shifts in the equilibrium branches without altering the critical delay at which the Hopf bifurcation occurs, confirming that the stability threshold is insensitive to changes in excitation magnitude. The combined influence of time delay τ and the control parameter γ on equilibrium stability is illustrated in Figure 7(c). Stable equilibrium solutions persist for small values of τ, while unstable solutions arise once the delay exceeds a critical threshold. Increasing γ leads to a pronounced reduction in the equilibrium amplitude and a significant enlargement of the stability region. This behavior indicates that higher values of γ effectively suppress delay-induced instabilities and enhance the robustness of the equilibrium state. Overall, these results demonstrate that while time delay plays a dominant role in triggering instability through Hopf bifurcation, appropriate tuning of the control parameter γ can substantially improve system stability and mitigate adverse dynamical effects associated with delayed feedback. Figure 8 depicts the transient responses of the controlled system for time-delay values $\tau = 0.5. 2.5$, and 4.6, respectively. A clear variation in control performance is observed as the delay increases. For $\tau = 0.5$, the response exhibits moderate vibration suppression, indicating partial control effectiveness. When $\tau = 2.5$, the system response rapidly converges to a low-amplitude steady state, which is consistent with operation on a stable equilibrium branch identified in Figure 6, demonstrating effective suppression of oscillations. In contrast, for $\tau = 4.6$, the response displays persistent oscillations or degraded attenuation performance, suggesting that this delay value lies within an unstable or weakly controlled regime. These results provide direct time-domain confirmation of the stability predictions presented in Figures 6 and 7 and highlight the critical influence of time delay on control effectiveness. To summarize the importance of time delay in system control, Figure 9 presents a comparative assessment of vibration suppression using negative acceleration feedback and negative delayed acceleration feedback. In comparison with the uncontrolled response, both control schemes lead to a substantial reduction in oscillation amplitude and a pronounced decrease in settling time. The negative delayed acceleration feedback demonstrates superior attenuation performance, which can be attributed to the phase shift introduced by the time delay, resulting in more efficient energy dissipation. Quantitatively, in the primary resonance condition, the effectiveness of the negative acceleration controller defined as $E_a = \frac{amplitudewithoutcontrol}{amplitudewithcontrol}$ is equal to 2. By incorporating delayed acceleration feedback, a higher level of damping is achieved, reducing the response amplitude to approximately 0.5. Consequently, the corresponding effectiveness increases to $E_a = 4$, confirming the enhanced vibration suppression capability of the delayed control strategy.

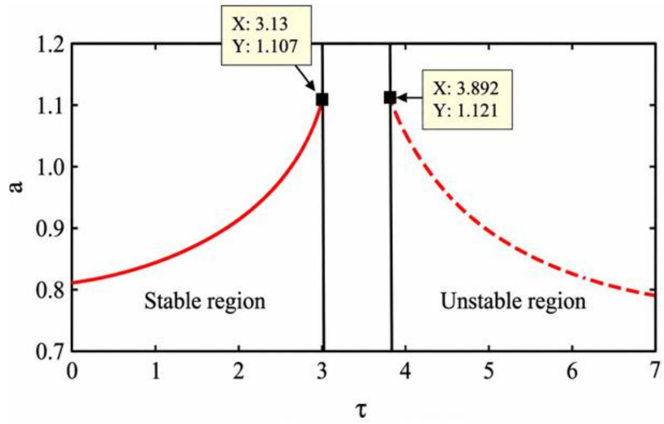

Figure 6. Stability and instability regions in the time-delay parameter space (τ).

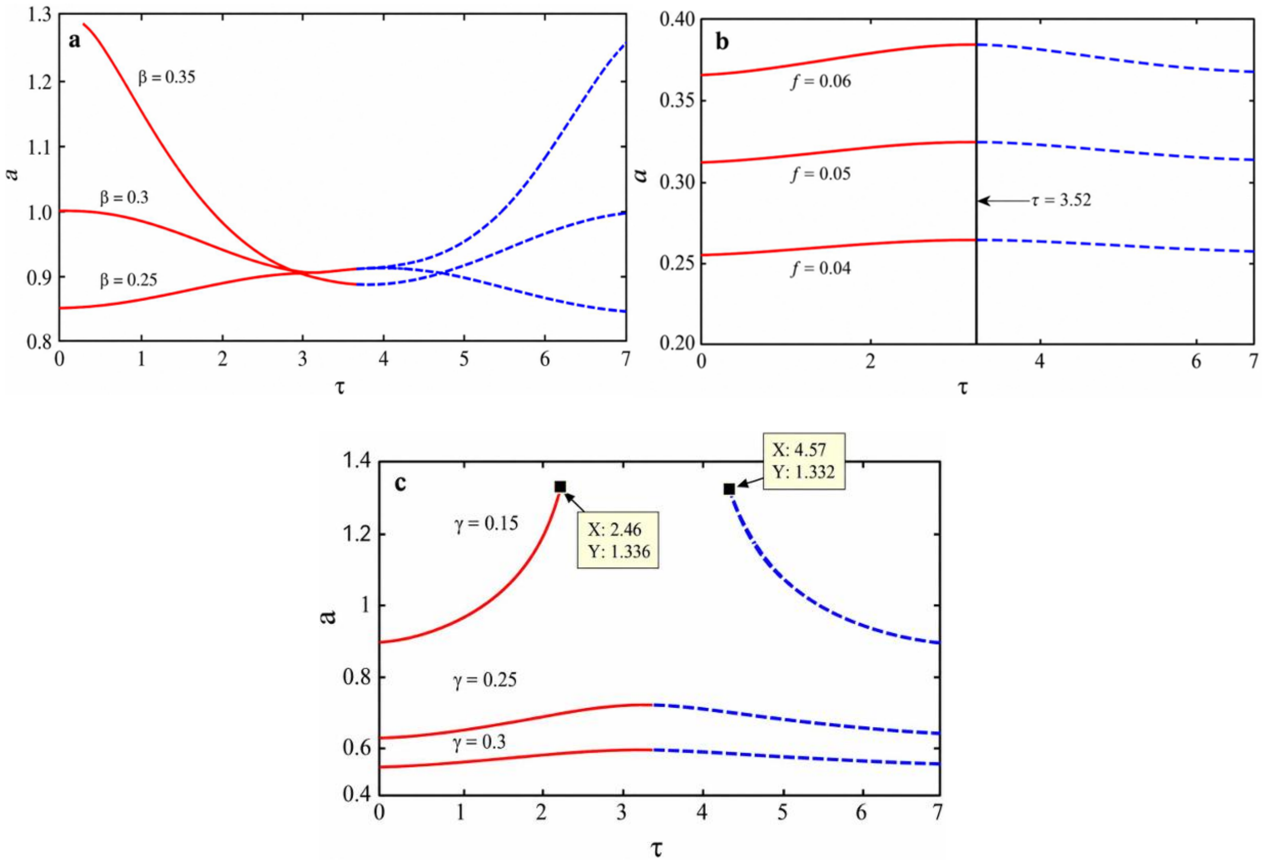

Figure 7. (a)–(c) Effects of the strength of the nonlinear rotating pendulum β, forcing amplitude f, and control parameter γ on the stability boundaries in the presence of time-delay acceleration feedback.

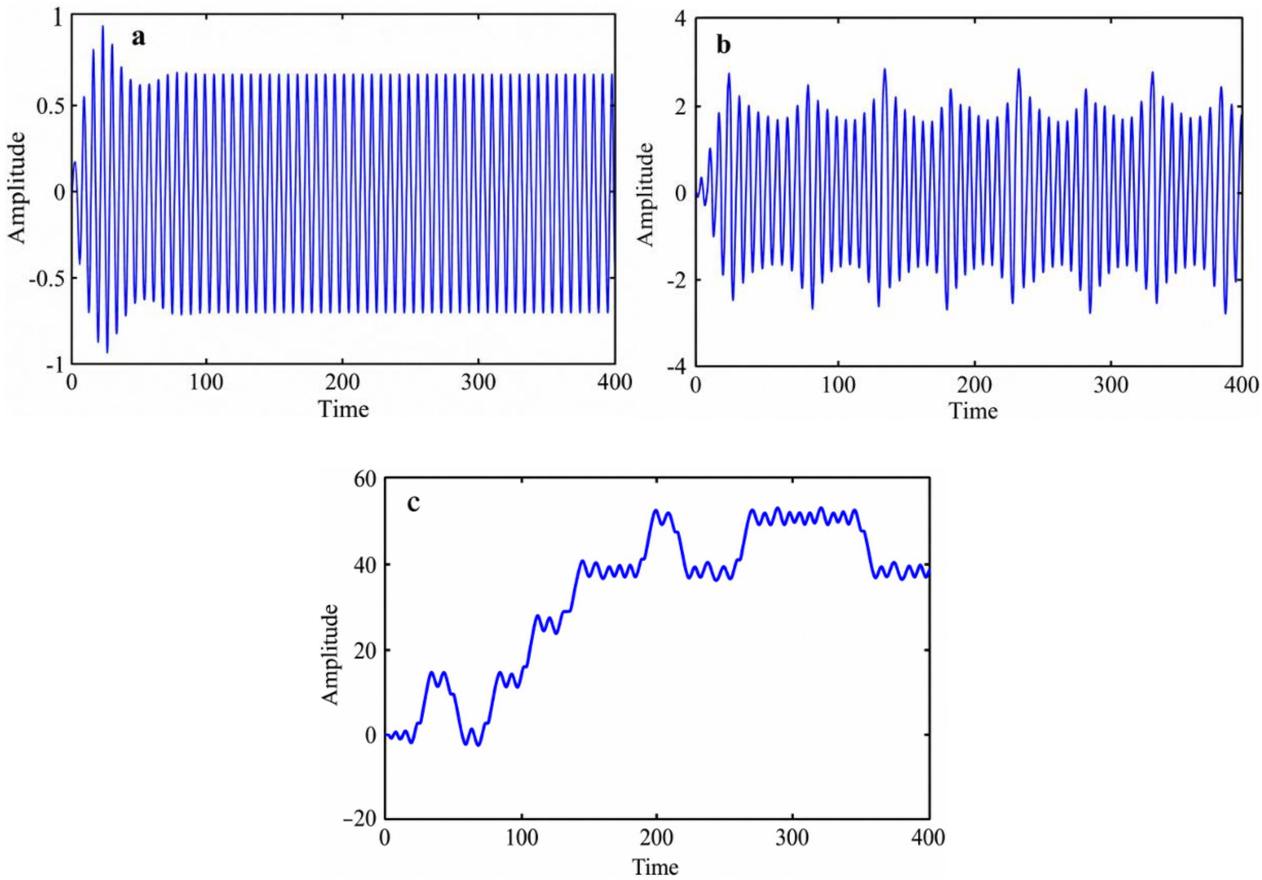

Figure 8. System response under negative delayed acceleration control at different values of time delay: (a) $\tau = 0.5$, (b) $\tau = 2.5$, and (c) $\tau = 4.6$.

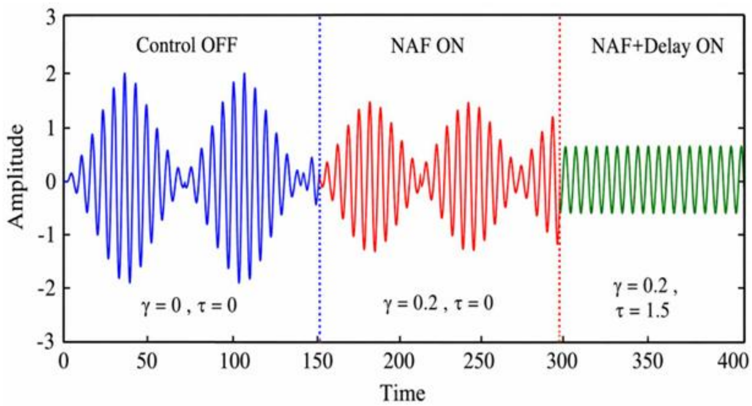

Figure 9. Comparison of vibration suppression using negative acceleration feedback and negative delayed acceleration feedback.

4.5. Validation of perturbation solutions via numerical results

This subsection compares numerical simulations with perturbation-based approximate solutions to validate the analytical approach. Results are presented for the uncontrolled system and for systems with negative acceleration and negative delayed acceleration control. Figure 10(a)–(c) shows the comparison between the numerical solutions (solid lines) and the perturbation-based approximate solutions (dashed lines) for the uncontrolled system, the system with negative acceleration control, and the system with negative delayed acceleration control, respectively. In all cases, the close agreement confirms the accuracy and validity of the analytical approximations. Panel (d) presents a direct comparison between the perturbation solution (solid blue curve) and the numerical results (green circles) across the detuning parameter σ. Excellent agreement is observed throughout, with both methods accurately capturing the resonance peak near $\sigma \approx 0$ and the amplitude attenuation away from resonance, demonstrating the robustness of the perturbation technique in predicting the steady-state response of the system.

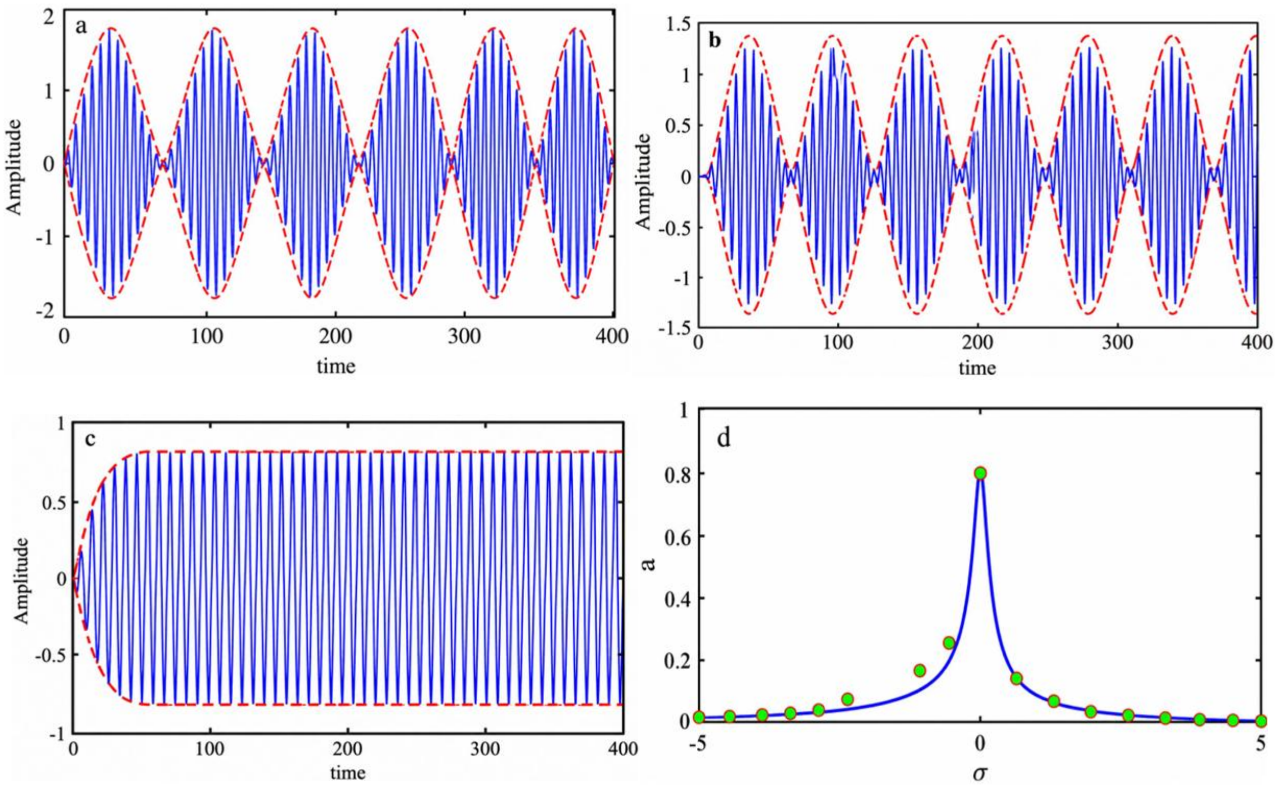

Figure 10. (a–c) Comparison of numerical and perturbation-based solutions for uncontrolled and controlled systems; (d) approximate solutions (blue) via numerical results (green circle).

5. Conclusions

Based on the analytical and numerical investigations of the nonlinear rotating pendulum subjected to a harmonic excitation force and delayed acceleration control, the following conclusions are drawn:

- Detuning parameter σ: The detuning parameter strongly governs the resonance behavior of the system. Maximum vibration amplitude occurs at primary resonance ($\sigma \approx 0$), while increasing $|\sigma|$ leads to rapid attenuation of the response. The amplitude–frequency curves exhibit symmetric behavior with respect to σ, reflecting the even-order dependence of the governing equations.

- Forcing amplitude f: Increasing the external forcing amplitude significantly raises the steady-state vibration amplitude and expands the multi-stability region. Higher values of f intensify nonlinear effects, enlarge the separation between fold points, and increase the likelihood of jump phenomena.
- Nonlinear modulation strength β: The parameter β plays a crucial role in shaping the system's nonlinear stiffness and resonance characteristics. Larger β values increase the peak response amplitude and shift stability boundaries toward smaller delay values, making the system more sensitive to delay-induced instability.
- Control gain γ: The control parameter γ has a pronounced stabilizing effect on the system. Increasing γ consistently reduces the vibration amplitude across the entire detuning range and enlarges the region of asymptotic stability. Higher γ values effectively suppress excessive oscillations and mitigate delay-induced instabilities.
- Time delay τ: Time delay critically influences system stability. Small delay values preserve asymptotic stability, while increasing τ can trigger Hopf bifurcations and lead to self-sustained oscillations. Distinct stable, transition, and unstable regions are identified, highlighting the dual roles of delayed feedback in both stabilizing and destabilizing systems.
- Moreover, numerical simulations based on the fourth-order Runge–Kutta method show excellent agreement with the perturbation-based analytical solutions. This agreement validates the accuracy of the multiple-scales approach in predicting steady-state response, resonance characteristics, and stability boundaries.

Author contributions

Khalid Alluhydan: Conceptualization, methodology, validation, formal analysis, investigation, resources, data curation, writing-original draft preparation, writing-review and editing, visualization, project administration, funding acquisition; M. N. Abd EL-Salam: Conceptualization, methodology, validation, formal analysis, investigation, resources, data curation, writing-original draft preparation, writing-review and editing, visualization, project administration. All authors have read and approved the final version of the manuscript for publication.

Use of Generative-AI tools declaration

The authors declare they have not used Artificial Intelligence (AI) tools in the creation of this article.

Funding

This research was funded by the Ongoing Research Funding program (ORF-2026-588), King Saud University, Riyadh, Saudi Arabia.

Acknowledgements

The authors extend their appreciation to the Ongoing Research Funding program (ORF-2026-588), King Saud University, Riyadh, Saudi Arabia.

Data availability

The datasets generated and used during this current study are available from the corresponding author.

Conflict of interest

The authors declare that they have no known competing financial interests or personal relationships that could have appeared to influence the work reported in this paper.

References

1. X. Xu, M. Wiercigroch, M. Cartmell, Rotating orbits of a parametrically-excited pendulum, *Chaos, Soliton Fract.*, **23** (2005), 1537–1548. https://doi.org/10.1016/j.chaos.2004.06.053
2. M. Lakshmanan, S. Rajasekar, *Nonlinear dynamics: Integrability, chaos and patterns*, Berlin, Heidelberg: Springer, 2003. https://doi.org/10.1007/978-3-642-55688-3
3. A. O. Belyakov, A. P. Seyranian, A. Luongo, Dynamics of the pendulum with periodically varying length, *Physica D*, **238** (2009), 1589–1597. https://doi.org/10.1016/j.physd.2009.04.015
4. M. Farkas, *Periodic motions*, New York: Springer, 1994. https://doi.org/10.1007/978-1-4757-4211-4
5. M. Colera, M. Pérez-Saborid, Numerical investigation of the effects of compressibility on the flutter of a cantilevered plate in an inviscid, subsonic, open flow, *J. Sound Vib.*, **423** (2018), 442–458. https://doi.org/10.1016/j.jsv.2018.01.041
6. A. H. Nayfeh, D. T. Mook, *Nonlinear oscillations*, Wiley, 1995. https://doi.org/10.1002/9783527617586
7. A. H. Nayfeh, *Perturbation methods*, Wiley, 2000. https://doi.org/10.1002/9783527617609
8. A. H. Nayfeh, B. Balachandran, *Applied nonlinear dynamics: Analytical, computational, and experimental methods*, New York: Wiley, 1995. https://doi.org/10.1002/9783527617548
9. R. H. Rand, *Lecture notes on nonlinear vibrations*, 2012.
10. P. Wahi, A. Chatterjee, Averaging oscillations with small fractional damping and delayed terms, *Nonlinear Dyn.*, **38** (2004), 3–22. https://doi.org/10.1007/s11071-004-3744-x
11. K. Wu, C. Ren, Y. Chen, Time-delay vibration reduction control of 3-DOF vehicle model with vehicle seat, *Appl. Sci.*, **11** (2021), 9426. https://doi.org/10.3390/app11209426
12. X. Sun, Y. Qu, F. Wang, J. Xu, Effects of time-delayed vibration absorber on bandwidth of beam for low broadband vibration suppression, *Appl. Math. Mech.*, **44** (2023), 1629–1650. https://doi.org/10.1007/s10483-023-3038-6
13. Y. Guo, G. F. Xu, C. Y. Duan, Research on time-delayed vibration reduction control of 1/4 vehicle semi-active suspension system with three degrees of freedom, *Adv. Mech. Eng.*, **16** (2024), 1–11. https://doi.org/10.1177/16878132241273541
14. W. Chu, C. Li, Z. Lyu, Vibration mitigation of flexible beams through boundary motion with enhanced time-delayed control, *Thin-Walled Struct.*, **210** (2025), 113056. https://doi.org/10.1016/j.tws.2025.113056

15. Y. A. Amer, A. T. El-Sayed, M. N. Abd EL-Salam, Position and velocity time delay for suppression vibrations of a hybrid rayleigh-van der pol-duffing oscillator, *Sound Vib.*, **54** (2020), 149–161. https://doi.org/10.32604/sv.2020.08469
16. N. A. Saeed, J. Awrejcewicz, M. A. Alkashif, M. S. Mohamed, 2D and 3D visualization for the static bifurcations and nonlinear oscillations of a self-excited system with time-delayed controller, *Symmetry*, **14** (2022), 621. https://doi.org/10.3390/sym14030621
17. H. S. Bauomy, A. T. El-Sayed, A time-delayed proportional-derivative controller for a dielectric elastomer circular membrane, *Chin. J. Phys.*, **84** (2023), 216–231. https://doi.org/10.1016/j.cjph.2022.11.004
18. W. Li, L. Zhang, J. Cao, A note on Turing–Hopf bifurcation in a diffusive Leslie–Gower model with weak Allee effect on prey and fear effect on predator, *Appl. Math. Lett.*, **172** (2026), 109741. https://doi.org/10.1016/j.aml.2025.109741
19. R. E. Abdullah, R. K. Hussein, Y. A. Amer, O. M. Khaled, M. I. Attia, A. M. Abd-Elal, et al., Nonlinear vibration reduction in vertical conveyor systems using a nonlinear integral negative derivative feedback controller, *AIMS Math.*, **10** (2025), 28129–28150. https://doi.org/10.3934/math.20251237
20. H. S. Bauomy, A. T. El-Sayed, Active control of a rectangular thin plate via negative acceleration feedback, *J. Comput. Nonlinear Dyn.*, **11** (2016), 041025. https://doi.org/10.1115/1.4033307
21. D. H. Yang, J. H. Shin, H. Lee, S. K. Kim, M. K. Kwak, Active vibration control of structure by active mass damper and multi-modal negative acceleration feedback control algorithm, *J. Sound Vib.*, **392** (2017), 18–30. https://doi.org/10.1016/j.jsv.2016.12.036
22. Z. Cui, X. Zhang, T. Lu, Resonance analysis and time-delay feedback controllability for a fractional horizontal nonlinear roller system, *AIMS Math.*, **9** (2024), 24832–24853. https://doi.org/10.3934/math.20241209
23. E. Kaslik, E. A. Kokovics, A. Rădulescu, Stability and bifurcations in Wilson-Cowan systems with distributed delays, and an application to basal ganglia interactions, *Commun. Nonlinear Sci. Numer. Simul.*, **104** (2022), 105984. https://doi.org/10.1016/j.cnsns.2021.105984
24. K. Mokni, H. Ali, B. Ghosh, M. Chaoui, Nonlinear dynamics of a Darwinian Ricker system with strong Allee effect and immigration, *Math. Comput. Simul.*, **229** (2025), 789–813, https://doi.org/10.1016/j.matcom.2024.10.017
25. S. Chatterjee, Vibration control by recursive time-delayed acceleration feedback, *J. Sound Vib.*, **317** (2008), 67–90. https://doi.org/10.1016/j.jsv.2008.03.020
26. Z. Wang, H. Hu, Q. Xu, G. Stepan, Effect of delay combinations on stability and Hopf bifurcation of an oscillator with acceleration-derivative feedback, *Int. J. Non-Linear Mech.*, **94** (2017), 392–399. https://doi.org/10.1016/j.ijnonlinmec.2016.10.008